The Astrophysical Journal Letters, 980:L39 (9pp), 2025 February 20 https://doi.org/10.3847/2041-8213/adb134


# Evidence for Variable Accretion onto PDS 70 c and Implications for Protoplanet Detections

Yifan Zhou[1], Brendan P. Bowler[2,3], Aniket Sanghi[4,22], Gabriel-Dominique Marleau[5,6,7], Shinsuke Takasao[8], Yuhiko Aoyama[9], Yasuhiro Hasegawa[10], Thanawuth Thanathibodee[11], Taichi Uyama[12], Jun Hashimoto[13,14,15], Kevin Wagner[16], Nuria Calvet[17], Dorian Demars[18], Ya-Lin Wu[19], Lauren I. Biddle[2], Sebastiaan Y. Haffert[20], and Marta L. Bryan[21]

[1] University of Virginia, 530 McCormick Road, Charlottesville, VA 22904, USA; yzhou@virginia.edu
[2] Department of Astronomy, University of Texas at Austin, 2515 Speedway Stop C1400, TX 78712, USA
[3] Department of Physics, University of California, Santa Barbara, Santa Barbara, CA 93106, USA
[4] Cahill Center for Astronomy and Astrophysics, California Institute of Technology, 1200 E. California Boulevard, MC 249-17, Pasadena, CA 91125, USA
[5] Max-Planck-Institut für Astronomie, Königstuhl 17, 69117 Heidelberg, Germany
[6] Fakultät für Physik, Universität Duisburg-Essen, Lotharstraße 1, 47057 Duisburg, Germany
[7] Physikalisches Institut, Universität Bern, Gesellschaftsstr. 6, 3012 Bern, Switzerland
[8] Department of Earth and Space Science, Graduate School of Science, Osaka University, Toyonaka, Osaka 560-0043, Japan
[9] School of Physics and Astronomy, Sun Yat-sen University, Zhuhai 519082, People's Republic of China
[10] Jet Propulsion Laboratory, California Institute of Technology, Pasadena, CA 91109, USA
[11] Department of Physics, Faculty of Science, Chulalongkorn University, 254 Phayathai Road, Pathumwan, Bangkok 10330, Thailand
[12] Department of Physics & Astronomy, California State University Northridge, Live Oak Hall, Room 1128, 18111 Nordhoff Street, Northridge, CA 91330, USA
[13] Astrobiology Center, National Institutes of Natural Sciences, 2-21-1 Osawa, Mitaka, Tokyo 181-8588, Japan
[14] Subaru Telescope, National Astronomical Observatory of Japan, Mitaka, Tokyo 181-8588, Japan
[15] Department of Astronomy, School of Science, Graduate University for Advanced Studies (SOKENDAI), Mitaka, Tokyo 181-8588, Japan
[16] Steward Observatory, University of Arizona, 933 N. Cherry Avenue, Tucson, AZ 89712, USA
[17] Department of Astronomy, University of Michigan, 323 West Hall, 1085 South University Avenue, Ann Arbor, MI 48109-1107, USA
[18] Université Grenoble Alpes, CNRS, IPAG, F-38000 Grenoble, France
[19] Department of Physics, National Taiwan Normal University, 88 Sec. 4, Tingzhou Road, Taipei 11677, Taiwan
[20] Leiden Observatory, Leiden University, Einsteinweg 55, Leiden 2333CC, The Netherlands
[21] Depart of Astronomy & Astrophysics, University of Toronto, 50 St George Street, Toronto, ON M5S 3H4, Canada
*Received 2024 December 12; revised 2025 January 18; accepted 2025 January 27; published 2025 February 18*

## Abstract

Understanding the processes of planet formation and accretion in young systems is essential to unraveling the initial conditions of planetary systems. The PDS 70 system, which hosts two directly imaged protoplanets, provides a unique laboratory for studying these phenomena, particularly through H$\alpha$ emission, a commonly used accretion tracer. We present multiepoch observations and examine the variability in accretion signatures within this system, focusing on PDS 70 b and c. Using Hubble Space Telescope narrowband H$\alpha$ imaging data taken in 2020 and 2024, we achieve high signal-to-noise ratio detections of these planets and reveal significant changes in H$\alpha$ flux. For PDS 70 c, the H$\alpha$ flux more than doubled between 2020 and 2024. The trend is consistent with the one identified in recently published MagAO-X data, further confirming that PDS 70 c has become significantly brighter in H$\alpha$ between 2023 March and 2024 May. The observed variability suggests dynamic accretion processes, possibly modulated by circumplanetary disk properties or transient accretion bursts. High-amplitude variability in PDS 70 c motivates simultaneous monitoring of multiple accretion tracers to probe the mechanisms of mass growth of gas giant planets. We quantify the impact of variability on the detectability of protoplanets in imaging surveys and emphasize the need for continued and regular monitoring to accurately assess the occurrence and characteristics of young, forming planets.

*Unified Astronomy Thesaurus concepts:* Exoplanet astronomy (486); Planet formation (1241); Direct imaging (387); Accretion (14); Time domain astronomy (2109)

*Materials only available in the online version of record: data behind figure*

## 1. Introduction

The PDS 70 system is among the most thoroughly studied sites of ongoing planet formation. This solar-mass star harbors two gas giants, PDS 70 b and c, located in the disk cavity (M. Keppler et al. 2018; S. Y. Haffert et al. 2019). The presence of a third planet has been suggested based on observations from Very Large Telescope (VLT) SPHERE and, more recently, JWST/NIRCam (D. Mesa et al. 2019; V. Christiaens et al. 2024). There is strong evidence suggesting ongoing mass accretion onto PDS 70 b and c (e.g., K. Wagner et al. 2018; S. Y. Haffert et al. 2019), most likely through their circumplanetary disks (A. Isella et al. 2019; M. Benisty et al. 2021). Additional signs suggest that gas and dust from the outer circumstellar disk are flowing into the disk cavity, fueling the growth of the two planets and replenishing the inner stellar disk (G. Perotti et al. 2023; V. Christiaens et al. 2024; E. Gaidos et al. 2024).

Accretion onto the PDS 70 planets is directly probed by the ultraviolet excess flux tracing the continuum of accretion shock

[22] NSF Graduate Research Fellow.

emission (Y. Zhou et al. 2021). However, the hydrogen recombination lines, H$\alpha$ in particular, are more regularly used in the investigation of the mass accretion rates of PDS 70 b and c (e.g., K. Wagner et al. 2018; S. Y. Haffert et al. 2019; J. Hashimoto et al. 2020; Y. Zhou et al. 2021), due to the more favorable observational circumstances in the optical bands for detecting H$\alpha$ than the Balmer continuum at these planets. H$\alpha$ emission may originate either from the accretion shock (Y. Aoyama et al. 2018; Y. Aoyama & M. Ikoma 2019) or from preshock gas in a magnetospheric accretion scenario similar to that of classical T Tauri stars (e.g., E. Gullbring et al. 1998; T. Thanathibodee et al. 2019). Depending on the assumed accretion models or scaling relations (e.g., A. Natta et al. 2004; J. M. Alcalá et al. 2017; Y. Aoyama et al. 2021), the estimated mass accretion rates of PDS 70 b and c range from $10^{-8}$ to $10^{-6}\,M_{\rm Jup}\,{\rm yr}^{-1}$ (e.g., K. Wagner et al. 2018; S. Y. Haffert et al. 2019; J. Hashimoto et al. 2020). In either scenario, most of the mass in these gas giant planets is expected to have already been accreted, since otherwise the current accretion rates could not support the formation of the two super-Jupiters within the age of the system (5.4 Myr; A. Müller et al. 2018).

The strong H$\alpha$ excess emission of the planets, when paired with the weak H$\alpha$ excess of the star, mitigates the brightness contrast challenge in direct imaging detections (e.g., L. M. Close et al. 2014; Y. Zhou et al. 2014). For PDS 70 b and c, the planet-to-star relative brightness in H$\alpha$ is greater than those in the $J/H/K$ bands and are comparable to those in the $L'$ band (S. Y. Haffert et al. 2019). Motivated by these findings, multiple H$\alpha$ high-contrast imaging surveys have been conducted to search for accreting (proto)planets but have largely yielded nondetections of young giant planets (G. Cugno et al. 2019; C. Xie et al. 2020; A. Zurlo et al. 2020). Interesting (proto)planetary candidates detected by infrared imaging (e.g., S. Sallum et al. 2015; T. Currie et al. 2022; I. Hammond et al. 2023; K. Wagner et al. 2023) or disk kinematic (e.g., R. Teague et al. 2018; C. Pinte et al. 2019, 2020) do not resemble PDS 70 b or c, i.e., these candidates are either not point sources or lack evidence of accretion (e.g., Y. Zhou et al. 2022). The low yields defy the expectation (C. Plunkett et al. 2024). Proposed explanations of the low detection rate of accreting planets include stringent requirements for circumplanetary disk formation (e.g., S. Sagynbayeva et al. 2024), extinction due to disk material (e.g., Y. Hasegawa et al. 2024), rarity of widely separated planets in general (e.g., B. P. Bowler 2016; E. L. Nielsen et al. 2019), and variability of the H$\alpha$ emission (S. D. Brittain et al. 2020).

Variability is a hallmark of accreting young stars and has been recently detected in accreting substellar companions (D. Demars et al. 2023). In accreting stars, variability manifests as rotation modulations caused by hot spots and stochastic variations associated with unstable mass flow (G. Costigan et al. 2014). Instabilities in the accretion process extend to the planetary regime, leading to predictions of variable accretion rate and luminosity in planetary accretion models (J. Szulágyi & B. Ercolano 2020; S. Takasao et al. 2021).

Are PDS 70 b and c rare or even unique outcomes of planet formation, or are these planets caught at a fortunate time when the accretion excess emission is especially high? Answers to these questions, which are critical for inferring the intrinsic population of forming gas giants, require monitoring the variability of these planets. Temporal variability in accreting planets also holds the key to the geometry of the accretion and mechanisms of mass growth.

Recently, L. M. Close et al. (2025) presented the first definitive evidence of H$\alpha$ variability in both PDS 70 b and c based on 3 yr of ground-based observations with MagAO-X. The H$\alpha$ luminosity of PDS 70 b decreased by a factor of 4.6 between 2022 March and 2023 March and then slightly rose by a factor of 1.6 between 2023 March and 2024 March. In contrast, PDS 70 c's H$\alpha$ luminosity increased by 2.3$\times$ between 2023 and 2024.

In this Letter, we present new observations of the PDS 70 system obtained with Hubble Space Telescope (HST) Wide Field Camera 3 (WFC3) with the F656N narrowband H$\alpha$ filter (Section 2). By combining these images with archival HST H$\alpha$ observations, we construct a data set with the longest total integration time and temporal coverage of PDS 70 at these wavelengths to date. This enables high signal-to-noise ratio (S/N) recoveries of PDS 70 b and c and reveals the transition disk in scattered light. Our analysis provides clear evidence of variable accretion onto the planets (Section 3) and places these findings within the broader context of protoplanet detection and planetary accretion processes (Section 4).

## 2. Observations and Data Reduction

We observed PDS 70 using the HST/WFC3 UVIS2 channel. Images were captured with the narrowband F656N filter ($\lambda_{\rm cen}$ = 6561.6 Å, width$_{\rm eff}$ = 17.65 Å) to measure the H$\alpha$ emission from the planetary system. The observations consisted of four visit sets, starting on UT 2024 April 8, 2024 April 10, 2024 April 12, and 2024 May 15. All images were collected prior to the telescope's transition to reduced gyro mode in 2024 June and, therefore, are not affected by the scheduling and roll angle flexibility of the telescope. The first visit set included six consecutive orbits, while the remaining three visit sets comprised two orbits. In three orbits (Orbits 4 and 5 in visit set 1 and Orbit 2 in visit set 2), the telescope failed to acquire the targets, and the corresponding data were discarded.[23] In total, nine orbits of successful observations have been completed, yielding 216 raw frames. Details of the observations are summarized in the Appendix.

The observing strategy followed the methods described in Y. Zhou et al. (2021). Specific techniques included four-point half-pixel dithering, Nyquist-sampled image reconstruction using Fourier interlacing (T. R. Lauer 1999), and multiroll angular differential imaging (ADI; e.g., G. Schneider et al. 1999; M. C. Liu 2004; C. Marois et al. 2006). The nine orbits of observations were carried out using six distinctive roll angles to facilitate ADI. The total integration time of 12,600 s in the F656N band was nearly 4 times the F656N data used in Y. Zhou et al. (2021), significantly improving the photometric sensitivity and precision.

Data reduction started with the `flc` files downloaded from the Mikulski Archive for Space Telescopes archive. Bad pixels and cosmic rays were initially flagged using the data quality array. Additional visual examination further identified spurious pixels that were not detected by the `Calwf3` pipeline. These pixels were replaced by bilinear interpolation of the neighboring pixels. Then, every set of four dithered images are combined into one following the procedures described in T. R. Lauer (1999) and Y. Zhou et al. (2021). The

[23] A repeat of these observations is scheduled in spring 2025.

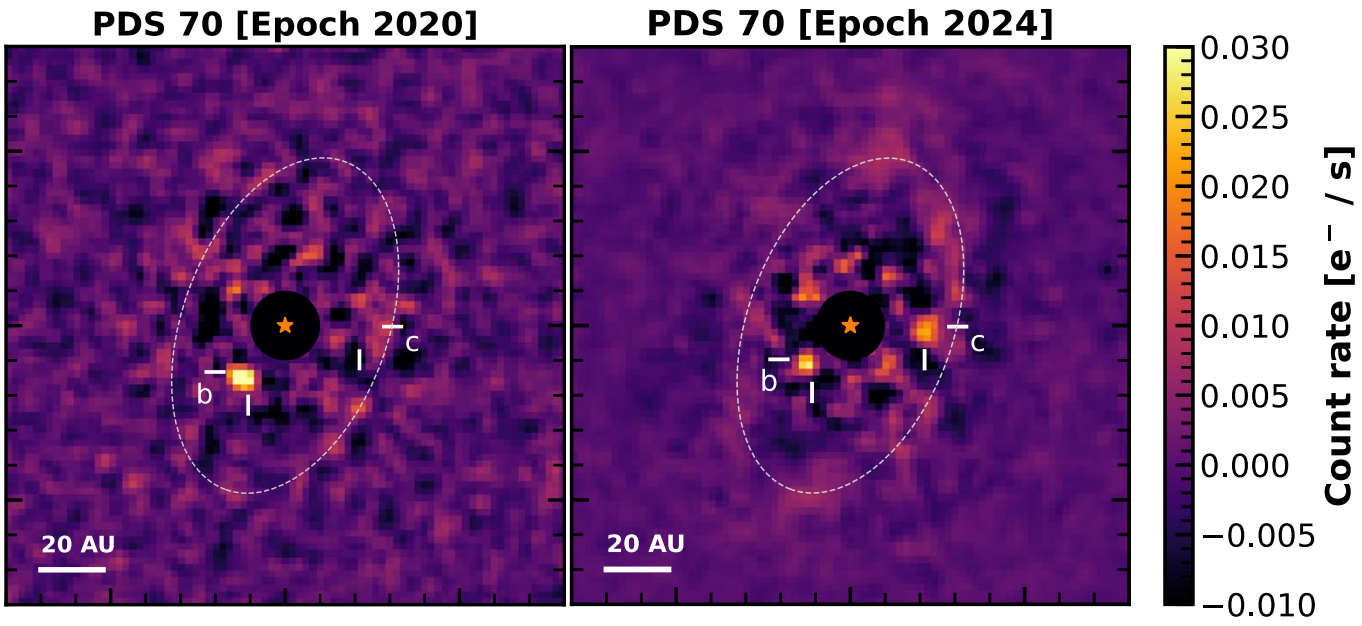


**Figure 1.** Primary-subtracted images of PDS 70 in 2020 (left) and 2024 (right). North is up and east is to the left. Color scales of the two panels are identical. The expected positions of PDS 70 b and c are marked. The white dashed line marks the inner edge of PDS 70's outer disk in infrared scattered light. PDS 70 b is detected in both epochs and demonstrates a significant orbital motion. PDS 70 c is only detected in Epoch 2024. The apparent brightness variations in PDS 70 b and c do not accurately represent the planets' intrinsic variability, as high-contrast imaging postprocessing introduces flux loss. For a comprehensive analysis of the evidence for variability, refer to Section 3.3.

(The data used to create this figure are available in the online article.)

reconstructed image has a pixel size of $0\farcs020$. Finally, geometric correction was conducted using the solution provided by A. Bellini et al. (2011).

We used the principal component analysis–based method implemented by the `pyKLIP` package to model and subtract the point-spread function (PSF) of the host star (R. Soummer et al. 2012). The ADI cube combines data taken in this observation (referred to as Epoch 2024) and data published in Y. Zhou et al. (2021; referred to as Epoch 2020). To aid in PSF modeling, an external reference star image library is formed using archival high-contrast images of several transition disk hosts that were observed using the same instrument set-ups obtained in program GO-16651. For the PSF modeling strategy, we have experimented with ADI, reference star differential imaging (RDI), and the combination of ADI and RDI (ADI + RDI). The ADI + RDI strategy was adopted because it delivered the deepest contrast. The `pyKLIP` control variables affecting the performance of PSF subtraction (b: `movement=3`, `subsection=3`, `annuli=15`, `numbasis=30`; c: `movement=3`, `subsection=1`, `annuli=15`, `numbasis=15`) were selected empirically, following the method detailed in J. I. Adams Redai et al. (2023). Images from Epochs 2020 and 2024 were combined into separate primary-subtracted images using inverse-variance-weighted averages (Figure 1).

The brightness of the star was measured using aperture photometry with a circular aperture of $r = 30$ pixels radius. The position and brightness of the two planets were determined by forward modeling (L. Pueyo 2016). The PSF representing the planet is created by the HST PSF modeling tool `Tiny Tim` (native pixel scale $= 0\farcs040$ pixel$^{-1}$; J. E. Krist et al. 2011) and then upsampled to a pixel scale of $0\farcs020$ pixel$^{-1}$ using the same method as applied to the observational data. Forward models were created by the `pyklip.fm` module. These models were then fit to the PSF-subtracted images, and the best-fitting parameters are determined by Markov Chain Monte Carlo (implemented by `emcee`; D. Foreman-Mackey et al. 2013). The means and standard deviations of the posterior chains were adopted as the best-fitting photometry and astrometry.

## 3. Results

### 3.1. The Recoveries of PDS 70 b and c

The primary-subtracted images reveal point sources located at the expected positions of PDS 70 b and c[24] (Figure 1). We evaluate the detection significance of the two planets using the S/N formula defined in D. Mawet et al. (2014). The Epoch 2020 image is consistent with that published by Y. Zhou et al. (2021). It does not show evidence of PDS 70 c but detects PDS 70 b with an S/N of 7. Both planets are present in the Epoch 2024 image. PDS 70 b is marginally detected with S/N = 4.0. PDS 70 c is more firmly recovered with S/N = 5.3.

The reduction in the detection S/N of PDS 70 b is due to its decreasing angular separation (see J. J. Wang et al. 2021b for the most up-to-date orbit solutions). The background noise at the location of PDS 70 b is dominated by speckles. Because of PDS 70 b's Keplerian motion on an inclined orbit, the angular separation of PDS 70 b decreases from 170 to 149 mas between the two observing epochs. This results in a significant increase in speckle noise and a more severe impact of ADI over- and self-subtraction in the latter epoch. Consequently, the detection confidence is lower in the more recent epoch.

[24] The planets' positions are estimated using http://whereistheplanet.com (J. J. Wang et al. 2021a). The orbit solution is provided by J. J. Wang et al. (2021b).

**Table 1**
Properties of PDS 70 b and c Constrained by the 2024 HST Epoch

| Planet | ΔR.A. (mas) | ΔDecl. (mas) | PA (deg) | Sep. (mas) | Count Rate ($e^- s^{-1}$) | F656N Flux ($10^{-16}$ erg s$^{-1}$ cm$^{-1}$) | $\log \dot{M}_{\rm Th19}$ ($M_{\rm Jup}$ yr$^{-1}$) | $\log \dot{M}_{\rm Ao21}$[a] ($M_{\rm Jup}$ yr$^{-1}$) |
|---|---|---|---|---|---|---|---|---|
| PDS 70 b | 110 ± 28 | −97 ± 24 | 131.4 ± 5.6 | 147 ± 28 | 1.30 ± 1.24[b] | 4.0 ± 3.7[b] | −8.0 | −7.5 |
| PDS 70 c | −213 ± 7 | −2.7 ± 6.5 | 213.5 ± 7.0 | 269.2 ± 1.7 | 2.41 ± 0.44 | 7.3 ± 1.3 | −8.0 | −7.6 |

**Notes.**
[a] We adopt planetary masses and radii of $M_{\rm b} = 3.2\,M_{\rm Jup}$, $M_{\rm c} = 7.5\,M_{\rm Jup}$, $R_{\rm b} = 2.0\,R_{\rm Jup}$, and $R_{\rm c} = 2.0\,R_{\rm Jup}$ (J. J. Wang et al. 2021b; D. Blakely et al. 2024).
[b] The flux uncertainties of PDS 70 b are strongly impacted by the fitting uncertainties in its positions and surrounding speckles. S/N values reported in Section 3.2 are calculated based on predetermined planet positions. Consequently, $f_{\rm b}/\Delta f_{\rm b} < {\rm S/N_b}$.

### 3.2. Astrometry and Photometry

The planetary signals are well fit by the forward models of the `Tiny Tim` point-source PSFs and do not show evidence of extended structures. Any self-subtraction between the planet PSFs is corrected by the forward-modeling process (L. Pueyo 2016). The MCMC fitting implemented by `pyklip.fm` converges to best-fitting values after the burn-in phase (200 steps). The posteriors of ΔR.A., Δdecl., and the scaling factors agree with normal distributions. Therefore, the mean and standard deviation values of the posteriors accurately represent the astrometry and photometry of the planets, as well as their associated uncertainties.

For both planets, the optical continuum flux emitted by their photospheres is negligible compared to that of the Hα line. Therefore, we assume all observed flux in the F656N filter is from the emission line. The observed count rate (in $e^- s^{-1}$) is converted to Hα flux by multiplying the conversion factor (`photflam2` header keyword) and the effective filter width ($W_{\rm eff} = 17.65$ Å). Table 1 lists the astrometry and photometry results. Mass accretion rates estimated using model-based scaling laws (Th19: T. Thanathibodee et al. 2019 and Ao21: Y. Aoyama et al. 2021) are also provided, which range from $\dot{M} \approx 1$ to $3 \times 10^{-8}\,M_{\rm Jup}\,{\rm yr}^{-1}$. These estimates are strongly model dependent and rely on loosely constrained masses and radii. We do not account for potential contamination of the Hα flux by stellar light reflected off the circumplanetary disks, which could lead to slight overestimation of the accretion rates.

### 3.3. Evidence for Variable Planetary Hα Flux

The recovered Hα flux of PDS 70 b and c differs from those reported in previous studies (S. Y. Haffert et al. 2019; J. Hashimoto et al. 2020; Y. Zhou et al. 2021). The 2024 flux of PDS 70 b ($f_{\rm b,2024} = (4.0 \pm 3.7) \times 10^{-16}$ erg s$^{-1}$ cm$^{-2}$) is less than one-quarter of the HST 2020 epoch flux ($f_{\rm b,2020} = (1.65 \pm 0.2) \times 10^{-15}$ erg s$^{-1}$ cm$^{-2}$). The 2024 flux of PDS 70 c ($f_{\rm c,2024} = (7.3 \pm 1.3) \times 10^{-16}$ erg s$^{-1}$ cm$^{-2}$) is more than twice its Hα flux ($f_{\rm c,MUSE} = (3.1 \pm 0.3) \times 10^{-16}$ erg s$^{-1}$ cm$^{-1}$) measured using VLT/MUSE data taken in 2018 (Figure 2). Variations in flux measurements between space- and ground-based observations may arise from the discrepancies in photometric calibration methods.

Forward-modeling photometry constrains the significance and amplitude of the variability signals. The Hα flux of PDS 70 b is not accurate enough to confirm its variability due to its close separation to the star in Epoch 2024 and the impact of self-subtraction. The variability of PDS 70 c can be precisely quantified. Figure 2 shows the marginal distribution of PDS 70 c flux constrained by the 2020 and 2024 data. The Epoch 2024 Hα flux of PDS 70 c ($f_{\rm c,2024} = (7.3 \pm 1.3) \times 10^{-16}$ erg s$^{-1}$ cm$^{-2}$) is $>3\sigma$ greater than the upper limit of the Epoch 2020 flux, defined as the 95th percentile of its posterior distribution ($f_{\rm c,2020} < 3.04 \times 10^{-16}$ erg s$^{-1}$ cm$^{-2}$). A 100% or greater increase in Hα flux is required to explain the difference between the two epoch images.

Injection-and-recovery tests further verify the variability signal. We inject synthetic PSFs that best fit to PDS 70 c in Epoch 2024 to the Epoch 2020 data. The injection location is first conducted at the expected position of PDS 70 c (PA = 276°, separation = 215 mas) and then repeated at four other locations with different PAs (10°, 80°, 220°, and 310°) and an identical separation (215 mas). All four injected signals are recovered with high confidence (S/N > 3, Figure 3). If PDS 70 c had a constant brightness, it should have been detected in the 2020 epoch.

Several of our data reductions show evidence for variability in PDS 70 b between 2020 and 2024, as well as in PDS 70 c between 2024 April and 2024 May; however, these variability signals strongly rely on the choice of `pyKLIP` control parameters. These low-significance variability signals are susceptible to over- or undersubtraction of stellar speckles (L. Pueyo 2016). For PDS 70 b, the uncertainties originate from the strong speckle noise at a close angular separation to the star. In the case of PDS 70 c, the detection of month-to-month variability is limited by the restricted variation in telescope orientation within each visit set. Currently, only the 2020 versus 2024 variability in PDS 70 c is robustly confirmed by our data. We defer the confirmation of the variability in PDS 70 b and short-cadence variability in PDS 70 c to future studies after the complete data set is collected in spring 2025.

### 3.4. Variable Hα Flux of the Host Star

The star PDS 70 also has variable Hα flux (Figure 4). The peak-to-peak flux change is over 40%, higher than that observed in the broad visible band (T. Thanathibodee et al. 2020). In Epoch 2024, the mean and standard deviation of the Hα flux are $f = 1.27 \times 10^{-12}$ and $1.31 \times 10^{-13}$ erg s$^{-1}$ cm$^{-2}$, respectively. The Epoch 2024 average flux is higher than that measured in Epoch 2020 ($f = 1.18 \times 10^{-12}$ erg s$^{-1}$ cm$^{-2}$), but the difference is less than $1\sigma$.

### 3.5. The Outer Disk of PDS 70 in Scattered Light

The Epoch 2024 image also detected the disk-scattered light. We estimate the location of the disk-scattered light and the possible contamination to the planet flux using the `diskfm` module of the `pyKLIP` package. For simplicity, a geometric disk model, following D. Blakely et al. (2024), is adopted over a radiative transfer model. The disk position angle and inclination are fixed to 160° and 53.°9 based on prior constraints

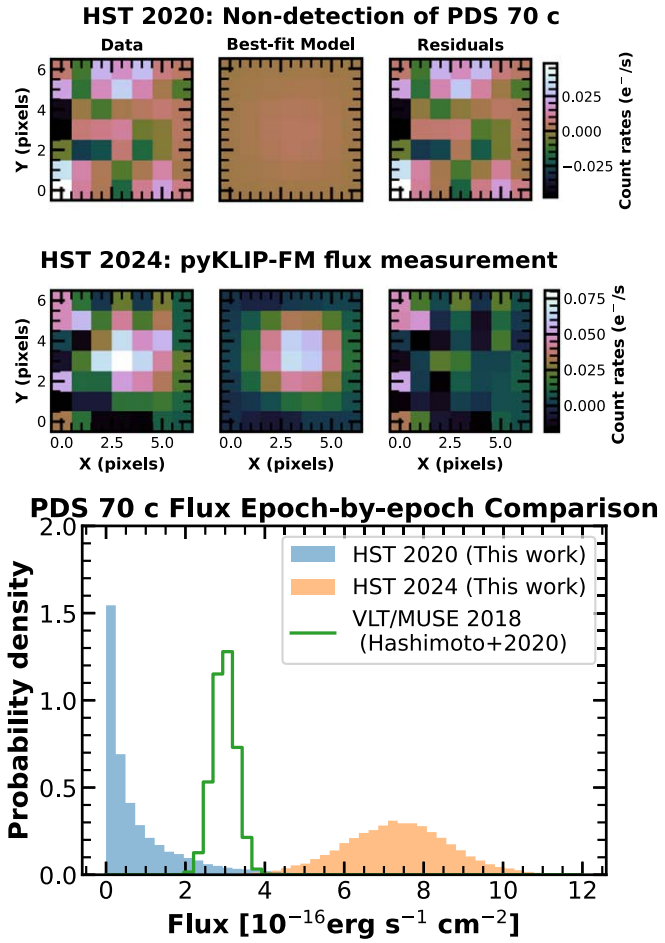


**Figure 2.** The variable H$\alpha$ flux of PDS 70 c. Top and middle rows: forward modeling at the expected positions of PDS 70 c in the 2020 and 2024 data. Both epochs consist of data collected spanning a few months (Table 2). The three panels (from left to right) are cutout data stamps centered at the planet, best-fit forward models, and fitting residuals, respectively. PDS 70 c is not detected in Epoch 2020, and the model in the top-middle row is consistent with zero flux. Bottom row: a comparison of PDS 70 c's H$\alpha$ flux measured in different epochs. Marginal posterior distributions of HST-based measurements are shown by filled histograms (blue and orange). The VLT/MUSE measurement ($f = (3.1 \pm 0.3) \times 10^{-16}$ erg s$^{-1}$ cm$^{-2}$; J. Hashimoto et al. 2020) is shown as a green solid line.

(e.g., M. Benisty et al. 2021; D. Blakely et al. 2024). We construct nine models to sample the peak deprojected radial location from 0.″34 to 0.″50. Each model comprises an axisymmetric component and an asymmetric component accounting for differences in scattering angle. The scalings of the model components are optimized to minimize the sum-squared residuals of pixels with deprojected distance between 40 and 80 au (0.″35 and 0.″70) away from the star. Two circular regions ($r = 0.''04$) centered at the planets are excluded from the residual calculations. The scattering light brightness is assumed to be constant over time.

Figure 5 presents the disk forward modeling results. A radius of $r = 0.''42$ disk minimizes the residuals. However, the disk flux is not completely eliminated by subtracting the best-fitting disk model, suggesting more complex disk structures than the geometric model. The radial peak is near the inner edge of continuum dust emission (e.g., M. Benisty et al. 2021) and slightly closer to the star than the one best-fitting to the infrared data (D. Blakely et al. 2024), suggesting micron-sized dust filtering into the transition disk gaps and trapped in pressure

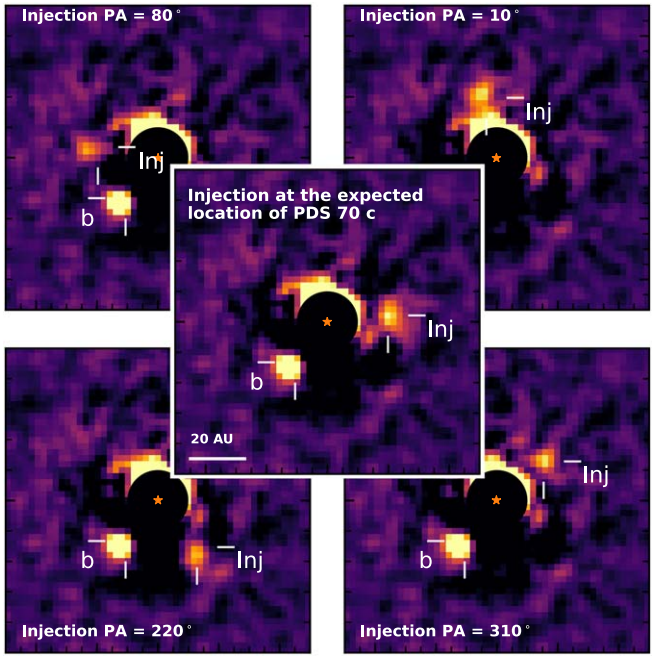


**Figure 3.** H$\alpha$ variability of PDS 70 c confirmed by injection/recovery tests. Point sources that have the same flux as PDS 70 c measured in Epoch 2024 are injected into the Epoch 2020 frames at the expected position of PDS 70 c (middle) and four different position angles. The injected planets are confidently recovered in all cases.

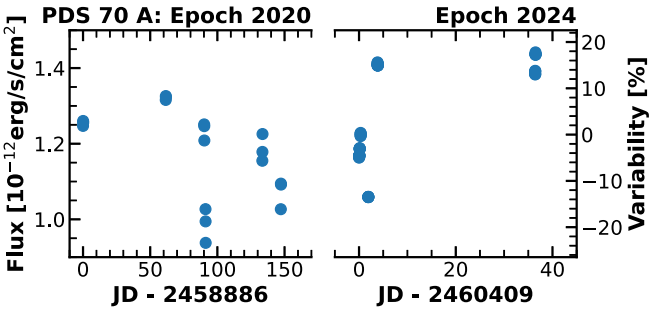


**Figure 4.** Variable H$\alpha$ flux emitted by the host star. Fluxes measured in Epoch 2020 and Epoch 2024 are shown as orange squares (left) and blue circles (right), respectively. Uncertainties are negligible (<1%) compared to the variability. Scales of absolute flux and relative changes are shown on the left and right axes, respectively. The variability is defined by the relative change over the median flux value.

bumps (e.g., P. Pinilla et al. 2018). The disk surface brightness measured at the positions of PDS 70 b and c is less than 0.002 e$^-$ s$^{-1}$. The disk contamination contributes less than 5% of the observed flux of PDS 70 b and c, negligible compared to the measurement uncertainties.

## 4. Discussion

### 4.1. A Comparison with the MagAO-X Results

The H$\alpha$ variability trends of PDS 70 b and c are consistently observed in both HST (this work) and MagAO-X (L. M. Close et al. 2025) data. Both data sets concur that PDS 70 b has dimmed, PDS 70 c has brightened, and PDS 70 c surpassed PDS 70 b in H$\alpha$ luminosity in 2024 March/April. It is important to note that the HST PDS 70 b measurement in Epoch 2024 is significantly affected by speckle noise and should be interpreted with caution.

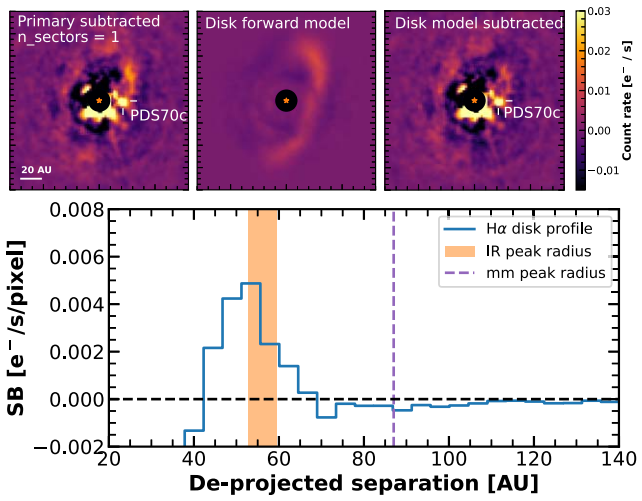


**Figure 5.** Estimations of the disk-scattered light emission (top panels) and the disk radial profiles (bottom panel). The top panels include a primary-subtracted image (left), the best-fitting model (middle), and the disk subtraction residuals. The primary subtraction was conducted using a relatively less aggressive strategy ($n_{\rm sector} = 1$, i.e., no subdivision within an annulus) to preserve disk flux. The H$\alpha$ scattered light of the disk can be reasonably well fit by a simple geometric model. In the radial direction, the disk's H$\alpha$ scattered light peaks at 50 au, slightly closer to the star than the disk seen in infrared. The disk surface brightness is low and has negligible contaminations to the planets' flux.

The observed H$\alpha$ brightening in PDS 70 c shows coincidentally similar amounts between this work (2.4×, between spring 2020 and spring 2024) and the MagAO-X results (2.3×, between 2023 March and 2024 March). The four visit sets of the 2024 HST observations (2024 April 8, 2024 April 10, 2024 April 12, and 2024 May 15) happened 2 to 7 weeks after the MagAO-X observation on 2024 March 25. The HST line flux exceeds the MagAO-X flux by 50% with a1.8$\sigma$ significance ($f_{\rm HST} = (7.3 \pm 1.3) \times 10^{-16}\,{\rm erg\,s^{-1}\,cm^{-2}}$, $f_{\rm MagAO\text{-}X} = (4.78 \pm 0.46) \times 10^{-16}\,{\rm erg\,s^{-1}\,cm^{-2}}$). This provides tentative evidence supporting short-term variability in PDS 70 c between 2024 March and May. However, systematic uncertainties due to differences in photometric calibrations between space and ground-based observations cannot be ruled out as the origin of the flux discrepancy.

L. M. Close et al. (2025) reported the detection of optical continuum flux at the position of PDS 70 b and attributed it to reflected stellar light from a circumplanetary disk. They suggested that this flux could contaminate the H$\alpha$ line flux and applied a correction factor of 1/1.54 to the HST Epoch 2020 flux when comparing the HST and MagAO-X photometry of PDS 70 b. Although no significant visible continuum flux has been detected near PDS 70 c, similar reflected light from PDS 70 c's disk might be obscured by speckle noise. Applying the same correction factor to our HST flux brings it consistent with the 2024 MagAO-X result.

### 4.2. Possible Origins of H$\alpha$ Variability

PDS 70 c's H$\alpha$ luminosity variability is within the range of that observed over year-long timescales in the Pa$\beta$ emission of the substellar companions GQ Lup b and GSC 06214 b (10–30 $M_{\rm Jup}$), as studied by D. Demars et al. (2023). The spectroscopically resolved hydrogen recombination lines observed at these objects provide evidence that they grow similarly to classical T Tauri stars by magnetospheric accretion (e.g., S. C. Ringqvist et al. 2023; G. Viswanath et al. 2024). T Tauri stars are variable over a wide range of timescales in the form of rotational modulations and various stochastic patterns (e.g., G. Costigan et al. 2014; G. Zsidi et al. 2022; G. J. Herczeg et al. 2023). If the variability observed in PDS 70 c has the same origin as the T Tauri stars, it must be in the long-term stochastic form because the observed variability timescale (a few years) is too long for rotational modulation. Indeed, the rotation period is expected to range from 10 to 20 hr down to less than 1 hr, nearly the breakup limit (see, e.g., M. L. Bryan et al. 2018; Y. Hasegawa et al. 2021). Then, the possible cause of the variability includes unstable interactions between the planet's magnetosphere and the circumplanetary disk (similar to those simulated for stars; see, e.g., A. K. Kulkarni & M. M. Romanova 2008; S. Takasao et al. 2022) or density fluctuations within the circumplanetary disk, whose Keplerian orbital timescale is less than 20 yr (estimated based on the disk size; M. Benisty et al. 2021).

Hydrogen line emission from the postshock gas, as opposed to the heated preshock gas in magnetospheric accretion, is also proposed as a scenario to model the accreting planets' H$\alpha$ emission (Y. Aoyama et al. 2018; Y. Aoyama & M. Ikoma 2019). A hydrodynamic model that couples accretion onto the disk and the planet suggests that the accretion shock at the planet's surface dominates the H$\alpha$ emission and that the accretion onto the disk triggers high-frequency (timescale $\ll$10 days), stochastic, and high-amplitude (order-of-magnitude) variability (S. Takasao et al. 2021). The detailed predictions could be sensitive to the details of the thermodynamics and the radiative transfer (G.-D. Marleau et al. 2023). The modeled H$\alpha$ luminosity smooths out over long timescales (>10 days). Testing the feasibility of the postshock gas emission in reproducing H$\alpha$ variability observed on year-long timescales requires extending the time length of existing models (e.g., S. Takasao et al. 2021).

Recently, V. Christiaens et al. (2024) identified a spiral-arm-like feature connecting PDS 70 c and the outer transition disk and interpreted it as a stream feeding the planet's disk. These findings draw parallels between accreting planets and protostars fed by streamers, in which interaction between the disk and the streamer flow triggers accretion outbursts (e.g., J. E. Pineda et al. 2020). JWST/NIRISS/AMI and NIRCam observations separated 12 days apart found a 75% (~3$\sigma$) discrepancy in the F480W flux of PDS 70 c (D. Blakely et al. 2024). If this difference is confirmed to trace variability of the circumplanetary disk (as against to instrumental or data-reduction-related systematic errors), this points to instability in the disk that may lead to the variability of accretion onto the planet.

Variations in line-of-sight extinction, potentially caused by micron-sized dust in the circumplanetary disk or by shielding from the accretion flow, can also drive the variability in H$\alpha$ flux (e.g., J. Szulágyi & B. Ercolano 2020; G. D. Marleau et al. 2022). A decrease of $\Delta A_V > 0.9$ mag in extinction can account for the observed >2× H$\alpha$ flux increase from 2020 to 2024. Simultaneous observations of accretion tracers in the visible and infrared bandpasses, even in the cases of nondetections, help constrain extinction level and test whether changing extinction is the source of H$\alpha$ variability (J. Hashimoto et al. 2020; T. Uyama et al. 2021).

By contributing to the planet's visible band flux through circumplanetary disk scattering, the stellar light may impact the observed variability of the planets (L. M. Close et al. 2025; see

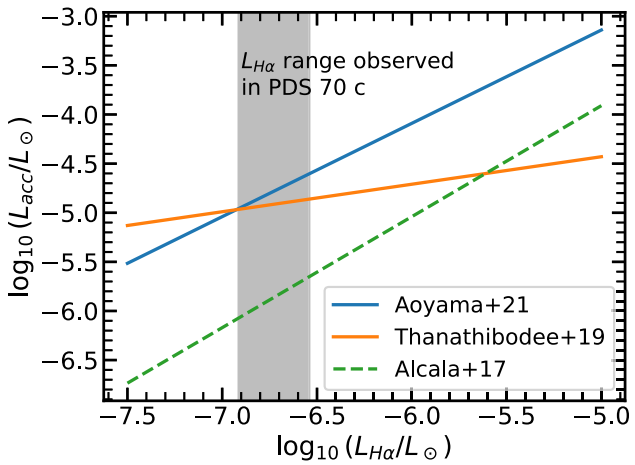


**Figure 6.** Comparisons of the $L_{acc}$–$L_{H\alpha}$ relationships near the observed $L_{H\alpha}$ of PDS 70 c. Predictions from the planetary accretion shock model (Y. Aoyama et al. 2021; blue solid line), the planetary magnetospheric model (T. Thanathibodee et al. 2019; orange solid line), and the empirical relation observed in T Tauri stars (J. M. Alcalá et al. 2017; green dashed line) are shown. The vertical gray region highlights the range of $L_{H\alpha}$ observed in PDS 70 c. Empirically mapping the $L_{acc}$–$L_{H\alpha}$ relationship in the PDS 70 planets will test these predictions.

also a light-echo experiment with the AB Aurigae system, B. P. Bowler et al. 2025). Variability of the host star between the 2020 and 2024 epochs (the epoch-to-epoch average flux difference is <10%) is too low to explain the significant variability observed in PDS 70 c. Future observations with improved cadence and sensitivity may distinguish the host star and planetary accretion–induced variability by identifying correlated changes between the planetary and stellar variability (B. P. Bowler et al. 2025).

### 4.3. Enabling an Empirical $L_{acc}$–$L_{H\alpha}$ Calibration for Accreting Planets

An important caveat is that these interpretations all rely on a correlation between the H$\alpha$ luminosity and the mass accretion rate. The H$\alpha$ emission from accreting stars often contains chromospheric components. The long-term monitoring of accreting low-mass stars show that the H$\alpha$ luminosity poorly constrains the accretion rate (G. J. Herczeg et al. 2023). The large-amplitude H$\alpha$ variability observed in PDS 70 c provides a new avenue to test the validity of $L_{H\alpha}$ in estimating the accretion rate if multiepoch H$\alpha$ and direct $L_{acc}$ measurements can be obtained. Testing the $L_{H\alpha}$–$L_{acc}$ on one planet avoids the inherent physical differences compared to other objects and isolates the origin of the H$\alpha$ emission and its luminosity variability.

Figure 6 shows the expected accretion luminosity variations with the changing H$\alpha$ luminosity. The assumed $L_{H\alpha}$–$L_{acc}$ relations, which include the prediction from the planetary strong shock model (Y. Aoyama et al. 2018, 2021), planetary magnetospheric model (T. Thanathibodee et al. 2019), and the empirical classic T Tauri star relation (J. M. Alcalá et al. 2017), differ significantly. Simultaneously monitoring PDS 70 b and c in multiple accretion tracers, which has been carried out for low-mass stars and substellar companions (e.g., S. K. Betti et al. 2022; Y. Aoyama et al. 2024; J. Hashimoto & Y. Aoyama 2025), will allow for a robust estimate of accretion luminosity variability. Then, the $L_{H\alpha}$–$L_{acc}$ relation observed in PDS 70 b and c informs their mass accretion mechanisms.

### 4.4. Implications about Detecting Accreting Planets

Variability of the H$\alpha$ emission is proposed as a possible solution to explain the low yield of accreting planet detections (e.g., S. D. Brittain et al. 2020). Our observations of PDS 70 c verify that the high-amplitude variability can critically impact the detectability of the planet. However, variability alone does not fully explain the lack of similar discoveries to PDS 70 b and c. Ground-based high-contrast H$\alpha$ imaging surveys have conducted over 50 unique observations on over 15 transition disk systems (C. Xie et al. 2020; A. Zurlo et al. 2020; K. B. Follette et al. 2023). Assuming all systems have at least one PDS 70 c-like planet and all planets have an identical accretion duty cycle, the accreting epoch must be very short such that the possibility of catching the planet while they are accreting is close to zero. This is incompatible with the successful H$\alpha$ recoveries of PDS 70 b and c in multiple epochs (K. Wagner et al. 2018; S. Y. Haffert et al. 2019; Y. Zhou et al. 2021, and this work). It is much more likely that PDS 70 bears unique disk and planetary properties that significantly enhance the direct detectability of the planets compared to other transition disk targets. Continued monitoring of PDS 70 c will help constrain the timescales and duty cycle of H$\alpha$ bursts, which is critical for accurately assessing imaging survey yields and estimating the occurrence rates and demographics of young gas giants.

## 5. Summary

Our main findings are the following:

1. We obtained new HST/WFC3/UVIS H$\alpha$ narrowband imaging data of the PDS 70 system and combined these data with a previous HST epoch taken in 2020. The new images have a 4 times longer integration time than the previous epoch, providing a more sensitive view of this site of planet formation. PDS 70 c and scattered light of the outer disk of PDS 70 are detected for the first time in HST H$\alpha$ images.
2. Planets PDS 70 b and PDS 70 c were recovered in the new images with S/Ns of 4.0 and 5.3, respectively. The positions of the two planets are consistent with those predicted by the latest orbit fitting solutions within their respective $1\sigma$ uncertainties.
3. Assuming all of the observed flux comes from the H$\alpha$ line emission, the H$\alpha$ line fluxes are $f = (4.0 \pm 3.7) \times 10^{-16}\,\mathrm{erg\,s^{-1}\,cm^{-2}}$ and $f = (7.3 \pm 1.3) \times 10^{-16}\,\mathrm{erg\,s^{-1}\,cm^{-2}}$ for b and c, respectively. The corresponding mass accretion rates are $\dot{M} \approx 1$ to $3 \times 10^{-8}\,M_{\rm Jup}\,\mathrm{yr^{-1}}$ based on scaling laws derived from planetary accretion models (T. Thanathibodee et al. 2019; Y. Aoyama et al. 2021).
4. The H$\alpha$ flux of PDS 70 c shows significant variability between Epoch 2020 and 2024. The Epoch 2024 flux is 2.4 times the upper limit (95 posterior percentile) obtained from the Epoch 2020 data ($>3\sigma$ confidence). The 2024 flux is also more than double the H$\alpha$ flux measured with 2018 VLT/MUSE data. Injection-and-recovery tests confirm the variability of PDS 70 c between the two HST epochs.

5. The H$\alpha$ flux of PDS 70 b measured in Epoch 2024 is less than 25% of its Epoch 2020 level reported by Y. Zhou et al. (2021). While this aligns with the the planet's decreasing H$\alpha$ luminosity determined using the MagAO-X data (L. M. Close et al. 2025), the strong speckle noise at PDS 70 b's Epoch 2024 location in the HST data prevents us from definitively confirming the variability in PDS 70 b.
6. The variability trends observed with HST are consistent with those observed with the ground-based MagAO-X instrument (L. M. Close et al. 2025). PDS 70 c's Epoch 2024 HST flux is $\sim$50% greater than that observed with MagAO-X a few weeks earlier, which tentatively indicate short-term variability. Confirming this variability requires calibrating space-based and ground-based high-contrast imaging photometry.
7. The nondetection of PDS 70 c in Epoch 2020 and its recovery in Epoch 2024 provides a concrete example where variable H$\alpha$ flux can impact the yields of protoplanetary imaging survey in the H$\alpha$ bandpass. However, H$\alpha$ variability is unlikely to be the sole reason for the low yields of (proto)planet searches. Future monitoring observations are necessary to determine the periodicity and duty cycle of the accretion activity. Estimating the yield of the imaging survey results should account for the variability flux to deliver unbiased population statistics of protoplanets.

## Acknowledgments

We acknowledge the anonymous referee for a prompt and constructive report that improved the manuscript. This work would not be possible without the excellent observation support from STScI Program Coordinator Amber Armstrong and Contact Scientist Joel Greene. This research is based on observations made with the NASA/ESA Hubble Space Telescope obtained from the Space Telescope Science Institute, which is operated by the Association of Universities for Research in Astronomy, Inc., under NASA contract NAS 5–26555. These observations are associated with programs GO-15830, GO-16651, and GO-17427. Y.Z. acknowledges HST data analysis grants associated with programs GO-15830, GO-16651, and GO-17427. This material is based upon work supported by the National Science Foundation Graduate Research Fellowship under grant No. 2139433. G.-D.M. acknowledges the support from the European Research Council (ERC) under the Horizon 2020 Framework Program via the ERC Advanced Grant "Origins" (PI: Henning), No. 832428, and via the research and innovation program "PROTOPLANETS," grant agreement No. 101002188 (PI: Benisty). S.T. was supported by JSPS KAKENHI grant Nos. JP21H04487, JP22K14074, and JP22KK0043. J.H. acknowledges the support from JSPS KAKENHI grant No. 23K03463. Y.H. was supported by the Jet Propulsion Laboratory, California Institute of Technology, under a contract with the National Aeronautics and Space Administration (80NM0018D0004).

*Software:* Astropy (Astropy Collaboration et al. 2013, 2018), SciPy (P. Virtanen et al. 2020), NumPy (C. R. Harris et al. 2020), Matplotlib (J. D. Hunter 2007), Seaborn (M. Waskom 2021), pyKLIP (J. J. Wang et al. 2015), emcee (D. Foreman-Mackey et al. 2013).

## Appendix
## Summary of HST High-contrast Observations of PDS 70

Information of HST observations of PDS 70 is summarized in Table 2. All observations are taken with WFC3/UVIS2 paired with the F656N filter. All data used in this Letter can be accessed at doi:10.17909/ndk6-9441.

**Table 2**
Observational Data Summary

| Visit Set | Beginning Time (UT) | End Time (UT) | Orbits | Position Angles (deg) | $N_{exp}$ | Total Exp. Time (s) |
|---|---|---|---|---|---|---|
| Epoch 2020, PID: 15830 | | | | | | |
| 1 | 2020-02-07 00:40:16 | 2020-02-07 04:29:40 | 3 | 100.8, 110.8, 120.8 | 27 | 540 |
| 2 | 2020-04-08 14:27:06 | 2020-04-08 18:19:53 | 3 | 140.8, 152.0, 163.0 | 27 | 540 |
| 3 | 2020-05-07 04:41:56 | 2020-05-07 08:33:35 | 3 | 181.0, 191.0, 201.0 | 27 | 540 |
| 4 | 2020-05-08 04:31:21 | 2020-05-08 08:23:00 | 3 | 211.0, 221.0, 231.0 | 27 | 540 |
| 5 | 2020-06-19 11:52:50 | 2020-06-19 15:44:29 | 3 | 259.1, 269.1, 279.1 | 27 | 540 |
| 6 | 2020-07-03 06:19:48 | 2020-07-03 10:06:19 | 3 | 279.1, 289.1, 297.1 | 27 | 540 |
| Epoch 2024, PID: 17427 | | | | | | |
| 1 | 2024-04-08 19:12:26 | 2024-04-09 03:40:00 | 6 | 135.3, 155.4 | 144 | 8448 |
| 2 | 2024-04-10 17:04:57 | 2024-04-10 19:23:33 | 2 | 136.9, 146.9 | 48 | 2880 |
| 3 | 2024-04-12 14:56:59 | 2024-04-12 17:15:34 | 2 | 139.6, 154.6 | 48 | 3000 |
| 4 | 2024-05-15 05:18:34 | 2024-05-15 07:38:59 | 2 | 216.6, 230.6 | 48 | 3120 |

## ORCID iDs

Yifan Zhou https://orcid.org/0000-0003-2969-6040
Brendan P. Bowler https://orcid.org/0000-0003-2649-2288
Aniket Sanghi https://orcid.org/0000-0002-1838-4757
Gabriel-Dominique Marleau https://orcid.org/0000-0002-2919-7500
Shinsuke Takasao https://orcid.org/0000-0003-3882-3945
Yuhiko Aoyama https://orcid.org/0000-0003-0568-9225
Yasuhiro Hasegawa https://orcid.org/0000-0002-9017-3663
Thanawuth Thanathibodee https://orcid.org/0000-0003-4507-1710
Taichi Uyama https://orcid.org/0000-0002-6879-3030
Jun Hashimoto https://orcid.org/0000-0002-3053-3575
Kevin Wagner https://orcid.org/0000-0002-4309-6343
Nuria Calvet https://orcid.org/0000-0002-3950-5386
Dorian Demars https://orcid.org/0009-0007-9582-553X
Ya-Lin Wu https://orcid.org/0000-0002-4392-1446
Lauren I. Biddle https://orcid.org/0000-0003-2646-3727
Sebastiaan Y. Haffert https://orcid.org/0000-0001-5130-9153
Marta L. Bryan https://orcid.org/0000-0002-6076-5967

## References

Adams Redai, J. I., Follette, K. B., Wang, J., et al. 2023, AJ, 165, 57
Alcalá, J. M., Manara, C. F., Natta, A., et al. 2017, A&A, 600, A20
Aoyama, Y., & Ikoma, M. 2019, ApJL, 885, L29
Aoyama, Y., Ikoma, M., & Tanigawa, T. 2018, ApJ, 866, 84
Aoyama, Y., Marleau, G.-D., & Hashimoto, J. 2024, AJ, 168, 155
Aoyama, Y., Marleau, G.-D., Ikoma, M., & Mordasini, C. 2021, ApJL, 917, L30
Astropy Collaboration, Price-Whelan, A. M., Sipőcz, B. M., et al. 2018, AJ, 156, 123
Astropy Collaboration, Robitaille, T. P., Tollerud, E. J., et al. 2013, A&A, 558, A33
Bellini, A., Anderson, J., & Bedin, L. R. 2011, PASP, 123, 622
Benisty, M., Bae, J., Facchini, S., et al. 2021, ApJL, 916, L2
Betti, S. K., Follette, K. B., Ward-Duong, K., et al. 2022, ApJL, 935, L18
Blakely, D., Johnstone, D., Cugno, G., et al. 2024, arXiv:2404.13032
Bowler, B. P. 2016, PASP, 128, 102001
Bowler, B. P., Zhou, Y., Biddle, L. I., et al. 2025, ApJ, submitted
Brittain, S. D., Najita, J. R., Dong, R., & Zhu, Z. 2020, ApJ, 895, 48
Bryan, M. L., Benneke, B., Knutson, H. A., Batygin, K., & Bowler, B. P. 2018, NatAs, 2, 138
Christiaens, V., Samland, M., Henning, T., et al. 2024, A&A, 685, L1
Close, L. M., Follette, K. B., Males, J. R., et al. 2014, ApJL, 781, L30
Close, L. M., Males, J. R., Li, J., et al. 2025, AJ, 169, 35
Costigan, G., Vink, J. S., Scholz, A., Ray, T., & Testi, L. 2014, MNRAS, 440, 3444
Cugno, G., Quanz, S. P., Hunziker, S., et al. 2019, A&A, 622, A156
Currie, T., Lawson, K., Schneider, G., et al. 2022, NatAs, 6, 751
Demars, D., Bonnefoy, M., Dougados, C., et al. 2023, A&A, 676, A123
Follette, K. B., Close, L. M., Males, J. R., et al. 2023, AJ, 165, 225
Foreman-Mackey, D., Hogg, D. W., Lang, D., & Goodman, J. 2013, PASP, 125, 306
Gaidos, E., Thanathibodee, T., Hoffman, A., et al. 2024, ApJ, 966, 167
Gullbring, E., Hartmann, L., Briceño, C., & Calvet, N. 1998, ApJ, 492, 323
Haffert, S. Y., Bohn, A. J., de Boer, J., et al. 2019, NatAs, 3, 749
Hammond, I., Christiaens, V., Price, D. J., et al. 2023, MNRAS, 522, L51
Harris, C.R., Millman, K. J., van der Walt, S. J., et al. 2020, Natur, 585, 357
Hasegawa, Y., Kanagawa, K. D., & Turner, N. J. 2021, ApJ, 923, 27
Hasegawa, Y., Uyama, T., Hashimoto, J., et al. 2024, AJ, 167, 105
Hashimoto, J., & Aoyama, Y. 2025, AJ, 169, 93
Hashimoto, J., Aoyama, Y., Konishi, M., et al. 2020, AJ, 159, 222
Herczeg, G. J., Chen, Y., Donati, J.-F., et al. 2023, ApJ, 956, 102
Hunter, J. D. 2007, CSE, 9, 90
Isella, A., Benisty, M., Teague, R., et al. 2019, ApJL, 879, L25
Keppler, M., Benisty, M., Müller, A., et al. 2018, A&A, 617, A44
Krist, J. E., Hook, R. N., & Stoehr, F. 2011, Proc. SPIE, 8127, 81270J
Kulkarni, A. K., & Romanova, M. M. 2008, MNRAS, 386, 673
Lauer, T. R. 1999, PASP, 111, 227
Liu, M. C. 2004, Sci, 305, 1442
Marleau, G. D., Aoyama, Y., Kuiper, R., et al. 2022, A&A, 657, A38
Marleau, G.-D., Kuiper, R., Béthune, W., & Mordasini, C. 2023, ApJ, 952, 89
Marois, C., Lafrenière, D., Doyon, R., Macintosh, B., & Nadeau, D. 2006, ApJ, 641, 556
Mawet, D., Milli, J., Wahhaj, Z., et al. 2014, ApJ, 792, 97
Mesa, D., Keppler, M., Cantalloube, F., et al. 2019, A&A, 632, A25
Müller, A., Keppler, M., Henning, T., et al. 2018, A&A, 617, L2
Natta, A., Testi, L., Muzerolle, J., et al. 2004, A&A, 424, 603
Nielsen, E. L., De Rosa, R. J., Macintosh, B., et al. 2019, AJ, 158, 13
Perotti, G., Christiaens, V., Henning, T., et al. 2023, Natur, 620, 516
Pineda, J. E., Segura-Cox, D., Caselli, P., et al. 2020, NatAs, 4, 1158
Pinilla, P., Benisty, M., de Boer, J., et al. 2018, ApJ, 868, 85
Pinte, C., Price, D. J., Ménard, F., et al. 2020, ApJL, 890, L9
Pinte, C., van der Plas, G., Ménard, F., et al. 2019, NatAs, 3, 1109
Plunkett, C., Follette, K. B., Marleau, G.-D., & Nielsen, E. 2024, arXiv:2408.01491
Pueyo, L. 2016, ApJ, 824, 117
Ringqvist, S. C., Viswanath, G., Aoyama, Y., et al. 2023, A&A, 669, L12
Sagynbayeva, S., Li, R., Kuznetsova, A., et al. 2024, arXiv:2410.14896
Sallum, S., Follette, K. B., Eisner, J. A., et al. 2015, Natur, 527, 342
Schneider, G., Smith, B. A., Becklin, E. E., et al. 1999, ApJL, 513, L127
Soummer, R., Pueyo, L., & Larkin, J. 2012, ApJL, 755, L28
Szulágyi, J., & Ercolano, B. 2020, ApJ, 902, 126
Takasao, S., Aoyama, Y., & Ikoma, M. 2021, ApJ, 921, 10
Takasao, S., Tomida, K., Iwasaki, K., & Suzuki, T. K. 2022, ApJ, 941, 73
Teague, R., Bae, J., Bergin, E. A., Birnstiel, T., & Foreman-Mackey, D. 2018, ApJL, 860, L12
Thanathibodee, T., Calvet, N., Bae, J., Muzerolle, J., & Hernández, R. F. 2019, ApJ, 885, 94
Thanathibodee, T., Molina, B., Calvet, N., et al. 2020, ApJ, 892, 81
Uyama, T., Xie, C., Aoyama, Y., et al. 2021, AJ, 162, 214
Virtanen, P., Gommers, R., Oliphant, T. E., et al. 2020, NatMe, 17, 261
Viswanath, G., Ringqvist, S. C., Demars, D., et al. 2024, A&A, 691, A64
Wagner, K., Follete, K. B., Close, L. M., et al. 2018, ApJL, 863, L8
Wagner, K., Stone, J., Skemer, A., et al. 2023, NatAs, 7, 1208
Wang, J. J., Kulikauskas, M., & Blunt, S. 2021a, whereistheplanet: Predicting Positions of Directly Imaged Companions, Astrophysics Source Code Library, ascl:2101.003
Wang, J. J., Ruffio, J.-B., De Rosa, R. J., et al. 2015, pyKLIP: PSF Subtraction for Exoplanets and Disks, Astrophysics Source Code Library, ascl:1506.001
Wang, J. J., Vigan, A., Lacour, S., et al. 2021b, AJ, 161, 148
Waskom, M., et al. 2021, JOSS, 6, 3021
Xie, C., Haffert, S. Y., de Boer, J., et al. 2020, A&A, 644, A149
Zhou, Y., Bowler, B. P., Wagner, K. R., et al. 2021, AJ, 161, 244
Zhou, Y., Herczeg, G. J., Kraus, A. L., Metchev, S., & Cruz, K. L. 2014, ApJL, 783, L17
Zhou, Y., Sanghi, A., Bowler, B. P., et al. 2022, ApJL, 934, L13
Zsidi, G., Fiorellino, E., Kóspál, Á., et al. 2022, ApJ, 941, 177
Zurlo, A., Cugno, G., Montesinos, M., et al. 2020, A&A, 633, A119